Exact Modeling of the Voltage Source Converter

P. W. Lehn, *Member, IEEE*

***Abstract*—A discrete time, linear time varying model of the three-phase voltage source converter (VSC) is developed. The model is employed to determine the steady-state operating characteristics of a VSC taking all ac–dc side harmonic interactions into account. The procedure is based on an exact closed form solution of the system equations and does not rely on iterative techniques. The steady-state operating curves from the proposed model are compared with those derived from a conventional continuous time dq-frame model. The accuracy of the conventional continuous time model is shown to be highly dependent on the converter's duty cycle.**

***Index Terms*—FACTS, modeling, power electronics, STATCOM, steady state analysis, VSC.**

I. Introduction

THE THREE-PHASE voltage source converter (VSC) is the basic building-block of most new FACTS and custom power equipment. The converter may be employed as a shunt compensator, series compensator or a hybrid compensator, as is the case with the unified power flow controller (UPFC) and the interline power flow controller (IPFC). Independent of the specific application, modeling is typically performed using an approximate continuous time representation of the converter in the synchronous reference frame [1], [2]. The continuous time model of the VSC yields an elegant set of three differential equations which represent the VSC operation with reasonable accuracy under most conditions.

There are, however, several limitations to this modeling approach. These include the inability to

1) represent the inherent discrete time nature of the VSC switching, which alone limits the closed loop performance of the VSC;
2) account for the effect harmonics have on the steady-state fundamental frequency behavior of the VSC;
3) model resonances, occurring between the ac and dc sides of the VSC, as well as those between the ac system and the VSC controls;
4) calculate ac and dc side harmonic injections generated by the converter switching.

Models based on time averaging theory have been proposed for both motor control and power supply applications [3], [4]. These models are exceptionally well suited for the development of converter controls because of their ability to represent the inherent discrete time nature of the VSC switchings. Contrary to what the name might imply, however, the time averaged models do not account for the effects that harmonics may have on the fundamental frequency behavior of the VSC. Limitations 2) through 4) are, therefore, not addressed by established time averaged models.

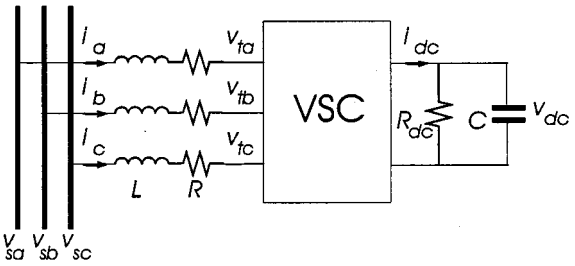

Fig. 1. The basic VSC circuit.

This paper presents a discrete time, linear time varying model of the basic three-phase VSC which avoids the time averaging assumption. Focus is on overcoming both limitations 1) and 2) by employing an exact analytical solution technique to obtain the steady-state behavior of the VSC, where all harmonic effects are taken into account. The exact solutions are compared with the approximate ones as obtained from a continuous time model [2]. It is demonstrated that the inclusion of harmonics can result in a significant shift in the fundamental frequency operation of the converter. Extension of the proposed modeling approach to address limitations 3) and 4) is under development.

II. Exact Linear Time Varying Model

Fig. 1 shows the basic three-phase VSC connected through an interface impedance to an infinite bus. This model is sufficient for representing most VSC applications, be they series, shunt or part of a hybrid connected device [1].

The VSC is modeled as a linear network with a topology that changes depending on the state of the six (ideal) switching devices. The linear time varying modeling techniques used to represent the VSC follows from basic theory presented in [5] and extended in [6]. The modeling approach exploits the fact that

- the system is piecewise linear;
- switchings occur at predefined times as determined by the VSC duty cycle and phase commands.

Consequently, over each interval during which the switches do not change their state, the circuit equations may be solved using standard linear techniques. Concatenating many such solutions permits the evolution of the state variables to be determined as a function of the switching times and the circuit's initial conditions. To employ this solution technique, the system differential equations must be expressed in either the abc or the $\alpha\beta$ reference frame. dq-frame modeling does not lend itself to

Manuscript received April 20, 2000.

The author is with the Department of Electrical and Computer Engineering, University of Toronto, Toronto, ON M5S 3G4, Canada.

Publisher Item Identifier S 0885-8977(02)00596-4.

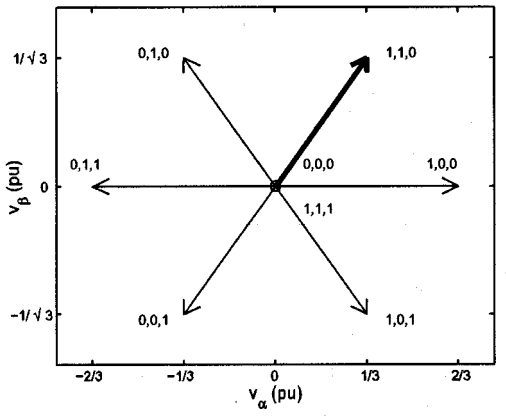

Fig. 2. Possible voltage space vectors.

such an approach since the dq-frame equations are not piecewise linear in nature. Modeling is carried out in the $\alpha\beta$-frame to exploit system symmetry. The transforms used are as follows:

$$\begin{bmatrix} v_\alpha \\ v_\beta \end{bmatrix} = \tfrac{2}{3}\mathbf{C_x}\begin{bmatrix} v_a \\ v_b \\ v_c \end{bmatrix} \quad \begin{bmatrix} i_\alpha \\ i_\beta \end{bmatrix} = \tfrac{2}{3}\mathbf{C_x}\begin{bmatrix} i_a \\ i_b \\ i_c \end{bmatrix} \tag{1}$$

$$\begin{bmatrix} v_a \\ v_b \\ v_c \end{bmatrix} = \mathbf{C_x}^T\begin{bmatrix} v_\alpha \\ v_\beta \end{bmatrix} \quad \begin{bmatrix} i_a \\ i_b \\ i_c \end{bmatrix} = \mathbf{C_x}^T\begin{bmatrix} i_\alpha \\ i_\beta \end{bmatrix} \tag{2}$$

where

$$\mathbf{C_x} = \begin{bmatrix} 1 & -\frac{1}{2} & -\frac{1}{2} \\ 0 & \frac{\sqrt{3}}{2} & -\frac{\sqrt{3}}{2} \end{bmatrix}. \tag{3}$$

Three unique gating signals control the three upper switches in a VSC while the lower switches are gated in a complimentary fashion. The three gating signals define the relationship between ac and dc side quantities [7].

The ac and dc side converter voltages are related by

$$\begin{bmatrix} v_{t\alpha} \\ v_{t\beta} \end{bmatrix} = \tfrac{2}{3}\mathbf{C_x}\begin{bmatrix} S_1 \\ S_2 \\ S_3 \end{bmatrix} v_{\rm dc} \tag{4}$$

where S_1, S_2, and S_3 represent the gating signals applied to the upper three switches. The gating signals are "1" when an upper switch is conducting and "0" when it is not. The lower switches are gated in a complementary fashion.

Eight possible gating combinations exist. Fig. 2 depicts the voltage space vector $\vec{v_t} = v_{t\alpha} + jv_{t\beta}$ associated with each of the eight gating combinations.

To illustrate, the switching function combination $\{S_1, S_2, S_3\} = \{1, 1, 0\}$ is associated with the vector in bold. The value of $v_{t\alpha}$ may then be read off the α-axis and the value of $v_{t\beta}$ may be read off the beta-axis. As shown in the figure, gating combinations $\{S_1, S_2, S_3\} = \{0, 0, 0\}$ and $\{S_1, S_2, S_3\} = \{1, 1, 1\}$ both yield the zero vector. These results are consistent with those obtained from space vector motor control theory [8]. The ac and dc side currents are related by

$$i_{\rm dc} = \begin{bmatrix} S_1 & S_2 & S_3 \end{bmatrix}\mathbf{C_x}^T\begin{bmatrix} i_\alpha \\ i_\beta \end{bmatrix}. \tag{5}$$

Employing these voltage and current relations, a set of linear differential equations can be derived for the VSC

$$\frac{d}{dt}\begin{bmatrix} i_\alpha \\ i_\beta \\ v_{\rm dc} \end{bmatrix} = \mathbf{A}_{S_1S_2S_3}\begin{bmatrix} i_\alpha \\ i_\beta \\ v_{\rm dc} \end{bmatrix} + \mathbf{N}\begin{bmatrix} v_{s\alpha} \\ v_{s\beta} \\ 0 \end{bmatrix} \tag{6}$$

with

$$\mathbf{A}_{S_1S_2S_3} = \begin{bmatrix} -\frac{R}{L} & 0 & -\frac{2}{3L}\mathbf{C_x}\begin{bmatrix} S_1 \\ S_2 \\ S_3 \end{bmatrix} \\ 0 & -\frac{R}{L} & \\ \frac{1}{C}\begin{bmatrix} S_1 & S_2 & S_3 \end{bmatrix}\mathbf{C_x}^T & & \frac{-1}{R_{\rm dc}C} \end{bmatrix} \tag{7}$$

$$\mathbf{N} = \begin{bmatrix} \frac{1}{L} & 0 \\ 0 & \frac{1}{L} \\ 0 & 0 \end{bmatrix}. \tag{8}$$

There are eight possible A matrices associated with the eight possible combinations of the gating signals S_1, S_2, and S_3. $\mathbf{A}_{111}$ and $\mathbf{A}_{000}$ are identical, however, as they are both associated with the same zero voltage space vector. Over any interval $t_0 < t < t_1$ during which no switchings occur, an exact solution to (6) exists, but it is difficult to evaluate. Assuming the system voltage contains only a fundamental frequency positive sequence component, the disturbance terms $v_{s\alpha}$ and $v_{s\beta}$ may be replaced with an ideal harmonic oscillator. This yields the following augmented set of differential equations

$$\frac{d}{dt}\begin{bmatrix} \mathbf{x} \\ z_1 \\ z_2 \end{bmatrix} = \begin{bmatrix} \mathbf{A}_{S_1S_2S_3} & \mathbf{N} & \\ \mathbf{0} & 0 & -\omega \\ & +\omega & 0 \end{bmatrix}\begin{bmatrix} \mathbf{x} \\ z_1 \\ z_2 \end{bmatrix} \tag{9}$$

where the initial conditions on the augmented state variables z_1 and z_2 contain the amplitude and phase information of the system voltage. (Note: the system voltage is related to the additional states according to $[v_{s\alpha} \quad v_{s\beta}]^T = [z_1 \quad z_2]^T$.) The augmented system equation (9) may be written in terms of an augmented state vector and system matrix as

$$\frac{d}{dt}\hat{\mathbf{x}} = \hat{\mathbf{A}}_{S_1S_2S_3}\hat{\mathbf{x}}. \tag{10}$$

Since the solution of the exact VSC equations depends on the switching methodology, a specific switching pattern must be specified before analysis may be carried out. For high-power applications two switching strategies are economically feasible:

- Type-I operation: switching at 3 or 9 times line frequency for independent control of dc voltage and reactive power compensation levels;
- Type-II operation: line frequency switching, yielding a dc voltage related to reactive power compensation level.

Analysis of the Type-I operation is carried out since Type-II operation may be considered a subclass of Type-I operation. For Type-I operation switching at three times line frequency, two possible switching strategies may be selected . To simplify

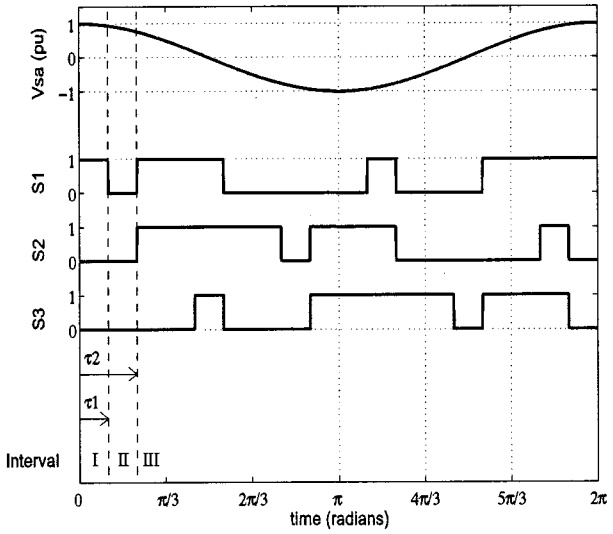

Fig. 3. Converter switching functions.

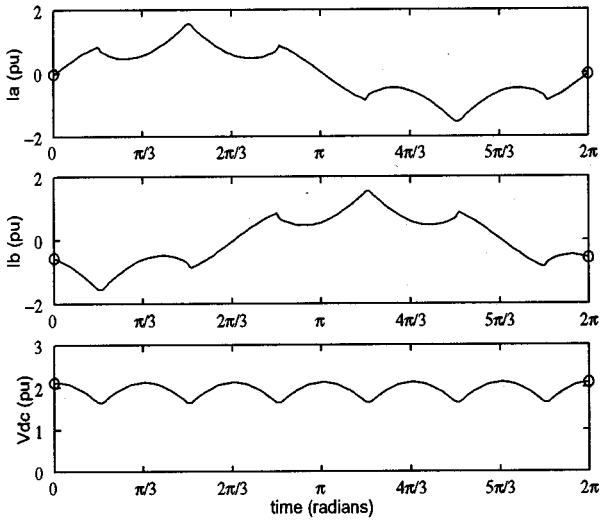

Fig. 4. Simulation of the converter in the steady state.

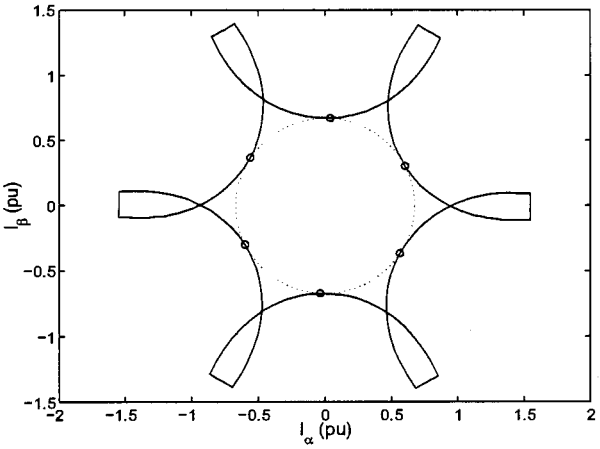

Fig. 5. Current space vector with one-sixth period symmetry.

analysis the switching functions used are those shown in Fig. 3. From the diagram it may be observed that Type-II operation occurs if the switching times τ_1 and τ_2 are set to the same value.

Fig. 3 is broken into six symmetrical 60° segments. (Symmetry may be identified by the fact that one switching function always has a notch, or a pulse, in the middle of each interval.) The symmetry is exploited in the analysis of the converter. Given the system state values at time $t = 0$, the solution for the states over the first sixth period is derived

$$\hat{\mathbf{x}}\left(\frac{\pi}{3}\right) = \hat{\mathbf{\Phi}}\hat{\mathbf{x}}(0) \tag{11}$$

where

$$\hat{\mathbf{\Phi}} = e^{\hat{\mathbf{A}}_{110}(\pi/3-\tau_2)} e^{\hat{\mathbf{A}}_{000}(\tau_2-\tau_1)} e^{\hat{\mathbf{A}}_{100}\tau_1}. \tag{12}$$

Using this formulation, the system may be accurately simulated to obtain the steady-state solution as shown in Fig. 4.

III. Steady-State Calculation

Steady state occurs when all the dc and ac quantities return to their initial values after one period, i.e.,

$$\hat{\mathbf{x}}_{ss}(2\pi) = \hat{\mathbf{x}}_{ss}(0). \tag{13}$$

This is indicated in Fig. 4 by the "O" markings. The rotation of the space vectors can be seen by plotting i_β versus i_α. Fig. 5 depicts the trajectory of the current space vector in the steady state. Inspection of the plot shows that no shorter period of symmetry shorter than 60° exists. Over the 60° interval the steady-state equations can be derived to be

$$\hat{\mathbf{x}}\left(\frac{\pi}{3}\right) = \hat{\mathbf{\Theta}}\hat{\mathbf{x}}(0) \tag{14}$$

where $\hat{\mathbf{\Theta}} = \mathrm{diag}(\mathbf{\Xi}, 1, \mathbf{\Xi})$ and $\mathbf{\Xi}$ is the 60° rotation matrix:

$$\mathbf{\Xi} = \begin{bmatrix} \cos\pi/3 & -\sin\pi/3 \\ \sin\pi/3 & \cos\pi/3 \end{bmatrix}. \tag{15}$$

Consequently, only a sixth period analysis is required to determine the steady-state operating point of the VSC. Imposing the steady-state constraint equation (13) on the dynamic solution equation (12) yields

$$\left(\hat{\mathbf{\Theta}} - \hat{\mathbf{\Phi}}\right)\hat{\mathbf{x}}_{ss}(0) = \mathbf{0}. \tag{16}$$

Partitioning this equation gives

$$\begin{bmatrix} \mathbf{E} & \mathbf{F} \\ \mathbf{G} & \mathbf{H} \end{bmatrix} \begin{bmatrix} \mathbf{x}_{ss}(0) \\ \mathbf{z}(0) \end{bmatrix} = \begin{bmatrix} \mathbf{0} \\ \mathbf{0} \end{bmatrix} \tag{17}$$

where $\mathbf{x}_{ss}(0)$ is the steady-state solution for the three original system states to be solved for. $\mathbf{z}(0)$ is the initial condition vector of the harmonic oscillator equations. It is a known vector which contains amplitude and phase information about the system voltage. The steady-state solution may then be found using standard linear techniques

$$\mathbf{x}_{ss}(0) = -\mathbf{E}^{-1}\mathbf{F}\mathbf{z}(0). \tag{18}$$

The steady-state solution gives the values of i_α, i_β, and v_{dc} at the specific time instant $t = 0$. At time $t = 0$ the system voltage

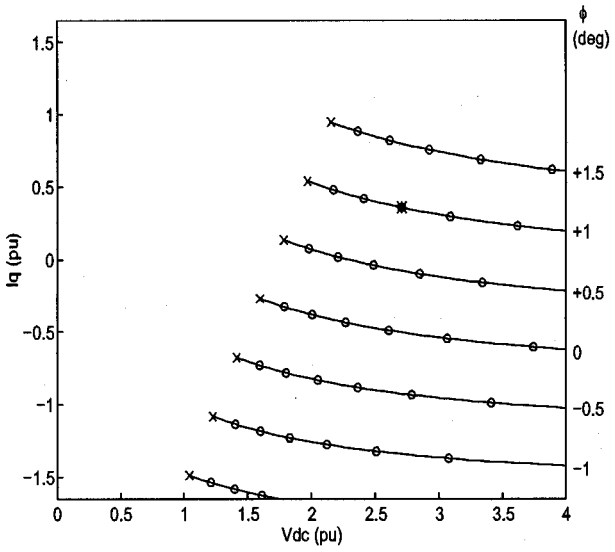

Fig. 6. Exact steady-state operating curves—sampled values.

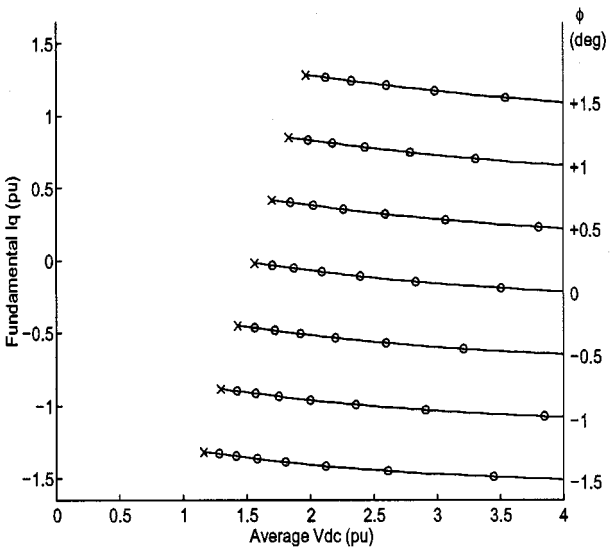

Fig. 7. Exact steady-state operating curves—fundamental components.

is assumed to be in-line with the α-axis and have an amplitude V_s. This specifies an initial condition vector $\mathbf{z}(0) = [V_s \;\; 0]^T$.

Although the presented analysis may only be carried out in the $\alpha\beta$-frame and not the dq-frame, at discrete instants in time the two reference frames coincide. This allows a dq-frame steady state to be extracted from the $\alpha\beta$-frame solution

$$\begin{bmatrix} i_{dss}(2n\pi) \\ i_{qss}(2n\pi) \end{bmatrix} = \begin{bmatrix} i_{\alpha ss}(2n\pi) \\ i_{\beta ss}(2n\pi) \end{bmatrix}, \quad \text{for } n = 0,\, 1,\, 2 \ldots. \tag{19}$$

A steady-state operating point may thus be calculated in terms of familiar d and q-axis quantities. Operating points are calculated as a function of the VSC duty cycle and phase angle. These quantities are related to the switching times τ_1 and τ_2 according to

$$D = 1 - \frac{\tau_2 - \tau_1}{\pi/3} \tag{20}$$

$$\phi = \frac{\tau_2 + \tau_1}{2} + \frac{\pi}{6}. \tag{21}$$

For STATCOM operation it is primarily the reactive current and dc voltage level that are of interest. The d-axis current will simply take on whatever value necessary to compensate losses occurring within the STATCOM. Associated with each set of controllable inputs D and ϕ, the steady-state dc voltage and ac currents may be calculated in closed form.

Fig. 6 depicts a family of steady-state operating curves plotted in the $v_{\rm dc}$–i_q state plane. Each curve corresponds to a fixed phase angle ϕ and a varying duty cycle D. At $D = 1$ pu the dc voltage takes on its minimum value on the curve, as indicated by the "X" markings. For each 0.1 pu decrement of the duty cycle an "O" is plotted on the curve. Thus for $\phi = +1^o$ (i.e., lagging the system voltage) and $D = 0.7$ pu, the steady-state operating point may be read off the plot to be $i_q = 0.36$ pu and $v_{\rm dc} = 2.7$ pu. This point is indicated by an asterisk in Fig. 6.

The system data used to generate Fig. 6, and all other operating curve diagrams, is given in the Appendix.

IV. Fundamental Frequency Solution

Analysis thus far has supplied curves which express the steady state in terms of its initial condition $\mathbf{x}_{ss}(0)$. This would correspond to the set of system state values at time $t = 0$ in Fig. 4 (left-hand set of "O" markings). To obtain both the average dc capacitor voltage and the fundamental frequency component of the VSC current, a Fourier analysis must be performed. The Fourier integrals may be solved using the method presented in [5] and extended in [6]. Over one sixth of a period, the dc voltage may be directly averaged

$$V_{\rm dc}^o = \frac{3}{\pi} \int_0^{\pi/3} v_{\rm dc}(t)\, dt. \tag{22}$$

The superscript "o" indicates the zeroth harmonic. To determine the positive sequence fundamental frequency component of the VSC current, a single complex Fourier integral can be evaluated

$$I^{+1} = \frac{3}{\pi} \int_0^{\pi/3} (i_\alpha(t) + j i_\beta(t)) e^{-jt}\, dt. \tag{23}$$

Operating curves are recalculated using the average dc voltage and the fundamental current. They are plotted in Fig. 7.

V. Approximate Continuous Time Model

The approximate continuous time VSC model typically employed for both steady-state and dynamic analysis is summarized in this section. A more complete discussion may be found in [2].

The approximate modeling approach neglects all switching operations occurring within the VSC and represents the converter as an ideal, lossless dc to (fundamental frequency) ac converter. Equating real powers on the two sides of the converter and expressing ac side quantities in the dq-reference frame yields a set of nonlinear, continuous time differential

TABLE I
INVERTER CONSTANTS FOR COMMON MODULATION SCHEMES

Modulation Scheme	Inverter Constant (k)
notched square wave	$2/\pi$
space vector	$1/\sqrt{3}$
sinusoidal PWM	$1/2$

equations. (The positive d-axis is along the positive x-axis, and the positive q-axis is along the positive y-axis.)

$$\frac{d}{dt}\begin{bmatrix} i_d \\ i_q \\ v_{\rm dc} \end{bmatrix} = \begin{bmatrix} -\frac{R}{L} & \omega & -\frac{k}{L}D\cos\phi \\ -\omega & -\frac{R}{L} & -\frac{k}{L}D\sin\phi \\ \frac{3k}{2C}D\cos\phi & \frac{3k}{2C}D\sin\phi & -\frac{1}{R_{\rm dc}C} \end{bmatrix} \begin{bmatrix} i_d \\ i_q \\ v_{\rm dc} \end{bmatrix} + \begin{bmatrix} \frac{1}{L} & 0 \\ 0 & \frac{1}{L} \end{bmatrix} \begin{bmatrix} v_{sd} \\ v_{sq} \end{bmatrix}. \quad (24)$$

The two input variables are the firing angle of the converter ϕ and a normalized duty cycle D. k is the inverter constant. It represents the ratio between the fundamental component of the line-to-neutral peak ac voltage and the dc voltage when the duty cycle is unity. The value of the inverter constant depends on the type of modulation used as indicated in Table I. An inverter constant of $k = 2/\pi$ is used to correspond with the notched square wave gating patterns of Fig. 3 analyzed in the preceding section.

For Type-I operation, the converter is switched at three times line frequency and the duty cycle may be varied between 0 and 1. For Type-II operation, the converter is switched at line frequency and the duty cycle is held constant at its maximum value.

Equating the left-hand side of equation (24) to zero and solving the resulting nonlinear equations as a function of duty cycle and phase angle, yields the system's steady-state solution as a function of the controllable inputs. To simplify the solution, the system voltage has been assumed to lie along the d-axis (i.e., $v_{sq} = 0$)

$$\begin{bmatrix} i_d \\ i_q \\ v_{\rm dc} \end{bmatrix} = \frac{v_{sd}}{\Delta}\begin{bmatrix} -2R - 3R_{\rm dc}k^2D^2\sin^2\phi \\ 2\omega L + 3R_{\rm dc}k^2D^2\sin\phi\cos\phi \\ 3(\omega LD\sin\phi - RD\cos\phi) \end{bmatrix}$$

$$\Delta = 2R^2 + 2\omega^2L^2 + 3D^2k^2R_{\rm dc}. \quad (25)$$

From the above equations the STATCOM operating curves may easily be drawn. They are depicted in Fig. 8.

VI. DISCUSSION OF RESULTS

The dq-frame model analyzed in the previous section yields steady-state operating curves assuming ideal ac to dc conversion. This results in total decoupling of the duty cycle and phase angle. Inspection of Fig. 8 shows that the reactive current level is controlled only by variations in the firing angle, while the duty cycle controls only the steady-state dc voltage level.

In contrast, the exact fundamental component curves of Fig. 7 demonstrate that such ideal decoupling does not actually exist

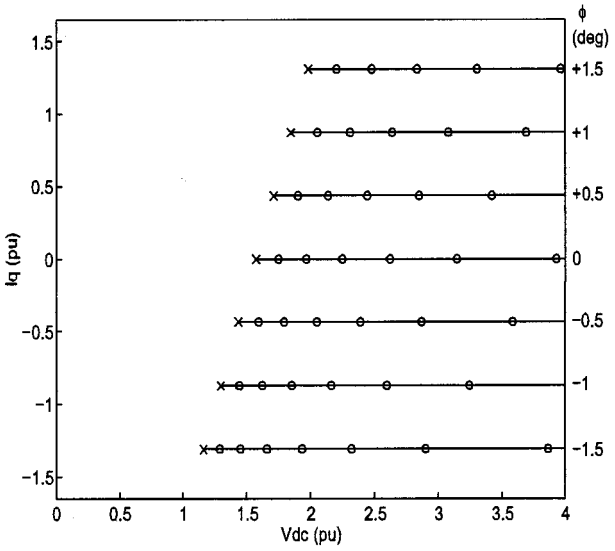

Fig. 8. Approximate steady-state operating curves.

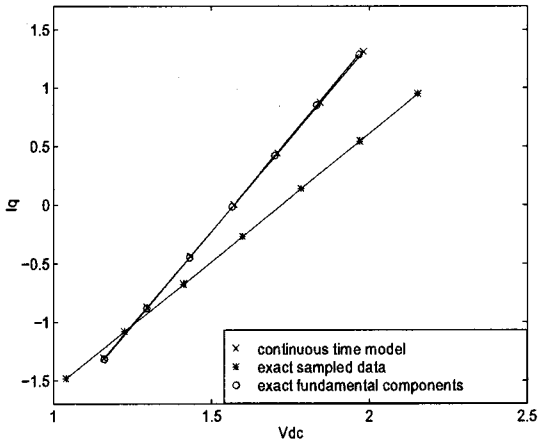

Fig. 9. Steady-state solutions for $D = 1$ pu.

if the converter switching is taken into account. This difference results from the presence of harmonic losses in the exact model, which are not represented in the approximate continuous time model. These harmonic losses disturb the delicate energy balance across the converter. Particularly when the converter is operated at high dc voltage levels, large harmonics result in the ac side current waveforms. These harmonics will cause additional real power to be dissipated in the interface inductance.

For extremely high power converters under Type-II operation, the duty cycle is continuously held at its maximum value of 1 pu. Operation of the converter in Type-II mode may be deduced from the operating curves by drawing a line through the "X" markings. Fig. 9 compares the various steady-state solutions when $D = 1$ pu. Under this mode of operation the approximate continuous time model is seen to produce nearly the same results as the one derived from fundamental frequency components in the exact model. The sample data solution from the exact model is also included for comparison. The sample data curve yields much higher dc voltage levels. This is because the samples are synchronized with the capacitor voltage harmonics (as seen in Fig. 4). This curve therefore yields the peak dc voltage, which is

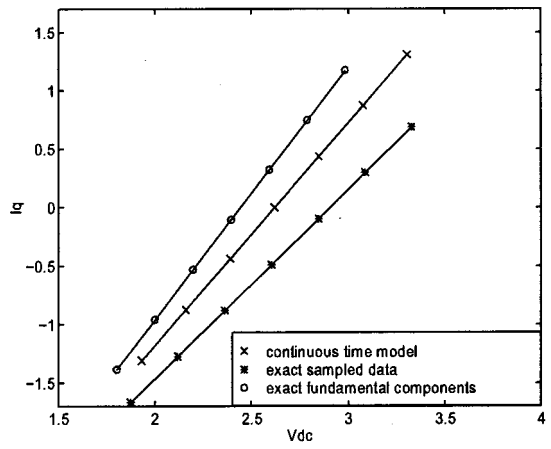

Fig. 10. Steady-state solutions for $D = 0.6$ pu.

significantly higher than the average dc voltage since a small dc side capacitor has been used. The sample data operating curves are also required for the design of high bandwidth digital VSC controllers.

For Type-I operation PWM is used. Depending on the reactive current reference, the duty cycle will vary between 1 pu down to as low as 0.6 pu. Fig. 10 compares the steady-state solutions for $D = 0.6$ pu. In contrast to the previous case, a large discrepancy now exists between the continuous time model and the exact fundamental frequency component solution. It may be concluded that the accuracy of the continuous time model drops significantly with reductions in the duty cycle.

VII. Conclusion

An exact VSC model has been developed based on a sample data representation of the system equations. The steady-state operating points of a VSC are found in closed form, as a function of the converter duty cycle and firing angle. Fourier analysis is applied in order to extract the fundamental frequency components associated with the steady-state operating points. Comparison of the proposed model with a conventional continuous time dq-frame VSC model shows that the continuous time model is highly accurate when the converter is operated with a duty cycle of 1 pu. As the duty cycle decreases, however, a significant error begins to develop in the continuous time model. This error results from the neglected harmonic components that can significantly shift the operating point of the VSC at lower duty cycles.

TABLE II
System Data

Quantity	Value
L	$0.20\ pu$
R	$0.02\ pu$
C	$0.50\ pu$
ω	$1.00\ pu$
R_{dc}	∞
$v_{sa}(peak)$	$1\ pu$

Appendix

The data used for the calculation of all operating curves is summarized in Table II. Individual switch resistances are included in the ac side resistance while switch forward voltage drops and switching losses are neglected.

References

[1] A. Sonnenmoser and P. Lehn, "Line current balancing with a unified power flow controller," *IEEE Trans. Power Delivery*, vol. 14, pp. 1151–1157, July 1999.
[2] C. Schauder and H. Mehta, "Vector analysis and control of advanced static VAR compensators," *Proc. Inst. Elect. Eng., pt. C*, vol. 140, pp. 299–306, July 1993.
[3] M. Depenbrock, "Direct self-control of inverter-fed induction machine," *IEEE Trans. Power Electron.*, vol. 3, pp. 420–429, Oct. 1988.
[4] P. Lehn and M. Iravani, "Discrete time modeling and control of the voltage source converter for improved disturbance rejection," *IEEE Trans. Power Electron.*, vol. 14, pp. 1028–1036, Nov. 1999.
[5] H. Visser and P. van den Bosch, "Modeling of periodically switched networks," in *Proc. IEEE PESC*, 1991, pp. 67–73.
[6] P. Lehn, "Modeling and control of switched circuits for high power applications," Ph.D. dissertation, Univ. Toronto, 1999.
[7] G. Séguier and F. Labrique, *Power Electronic Converters: DCAC Conversion*. New York: Springer-Verlag, 1993.
[8] P. Vas, *Vector Control of AC Machines*. New York: Oxford Univ. Press, 1990.

P. W. Lehn (S'95–M'99) received the B.Sc. and M.Sc. degrees in electrical engineering from the University of Manitoba, Canada, in 1990 and 1992, respectively. He received the Ph.D. degree from the University of Toronto, Canada, in 1999.

From 1992 until 1994 he waswith the Network Planning Group, Siemens AG, Erlangen, Germany. Presently, he is an Assistant Professor at the University of Toronto.